

Graphene Oxide Templated Growth and Superior Lithium Storage Performance of Novel Hierarchical $\text{Co}_2\text{V}_2\text{O}_7$ Nanosheets

Yanzhu Luo,^{†,||} Xu Xu,^{†,‡,||} Yuxiang Zhang,[§] Chih-Yen Chen,[‡] Liang Zhou,[†] Mengyu Yan,[†] Qiulong Wei,[†] Xiaocong Tian,[†] and Liqiang Mai^{*,†}

[†]State Key Laboratory of Advanced Technology for Materials Synthesis and Processing, Wuhan University of Technology, Wuhan 430070, People's Republic of China

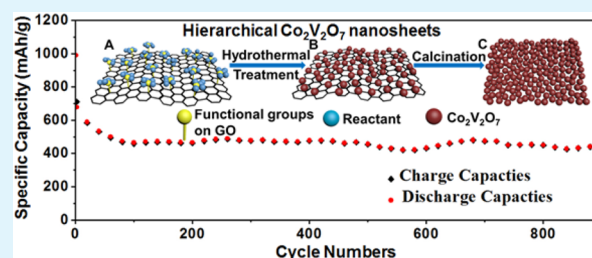
[‡]Department of Chemistry and Biochemistry, University of California, Los Angeles, California 90095, United States

[§]WUT Powerful Energy Co., Ltd., Wuhan 430223, People's Republic of China

S Supporting Information

ABSTRACT: Hierarchical $\text{Co}_2\text{V}_2\text{O}_7$ nanosheets consisted of interconnected nanoparticles are synthesized by a facile method using graphene oxide as the template. The electrochemical reaction mechanism of the $\text{Co}_2\text{V}_2\text{O}_7$ nanosheets is thoroughly investigated by in situ XRD and ex situ TEM. The initial $\text{Co}_2\text{V}_2\text{O}_7$ transforms into CoO nanoparticles and vanadium oxides in the first cycle, and the following reversible conversion reaction mainly occurs between CoO and Co and lithiation/delithiation of the vanadium oxides. The $\text{Co}_2\text{V}_2\text{O}_7$ nanosheet displays a high reversible capacity (962 mAh/g at 0.5 A/g) and remarkable high rate capability. When cycled at 5.0 A/g, a reversible capacity of 441 mAh/g can be retained after 900 cycles. The stable high capacity and excellent rate capability make the hierarchical $\text{Co}_2\text{V}_2\text{O}_7$ nanosheets a promising anode material for lithium-ion batteries.

KEYWORDS: cobalt vanadium oxide, hierarchical structure, lithium-ion battery, lithium storage mechanism, graphene oxide



1. INTRODUCTION

With the surge of portable electronics, electric vehicles, and large-scale power-grid storage, lithium-ion batteries (LIBs) with high energy/power densities and long cycle life have attracted great attention.^{1–4} The development of high-performance LIBs ultimately depends on the electrode materials.⁵ However, the traditional carbon-based anode materials exhibit a low specific capacity (theoretically 372 mAh/g for graphite) and serious safety issues.^{6–8} To meet the growing demand, transition metal oxides (MO_x , $M = \text{Co}, \text{Fe}, \text{Cu}, \text{Mn}, \text{etc.}$), which typically show theoretical capacity over 600 mAh/g, have been widely studied as promising alternatives to the conventional graphite anode.^{9–16} Among these candidates, cobalt oxides, in particular CoO and Co_3O_4 , have drawn particular attention due to their high theoretical Li-ion storage capacity.^{9,12,17–19} However, they suffer from poor conductivity and huge volume change during discharge/charge processes.

To address these issues, researchers have developed binary metal oxides as possible anode materials which can potentially synergistically enhance the electronic/ionic conductivity, reversible capacity, and mechanical stability.^{20–24} Furthermore, the partial replacement of expensive and toxic cobalt would make the materials cheaper and more eco-friendly.²⁰ Vanadium has been successfully employed to couple with cobalt, forming binary cobalt vanadates with desirable electrochemical performances. For example, the $\text{Co}_3\text{V}_2\text{O}_8$ multilayered nanosheets are capable of delivering a specific capacity of 1114 mAh/g over

100 cycles at 1.0 A/g. As another important cobalt vanadate, $\text{Co}_2\text{V}_2\text{O}_7$ can take up 13.6 Li ions in the voltage range of 0.02–3.5 V during the first discharge process, a little less than 15.4 Li ions for $\text{Co}_3\text{V}_2\text{O}_8$.²⁵ This means even with one more Co atom, $\text{Co}_3\text{V}_2\text{O}_8$ only provides 13% higher Li-storage capability than $\text{Co}_2\text{V}_2\text{O}_7$. Based on this, the research of $\text{Co}_2\text{V}_2\text{O}_7$ anode is worth being carried out as it contains lower cobalt content than $\text{Co}_3\text{V}_2\text{O}_8$, which means cheaper and more eco-friendly.

For the past few years, efforts have been devoted to improve the electrochemical performance of $\text{Co}_2\text{V}_2\text{O}_7$.^{25–28} Wu and co-workers have synthesized the mesoporous $\text{Co}_2\text{V}_2\text{O}_7$ mono-disperse hexagonal nanoplatelets, which display a high reversible capacity of 866 mAh/g after 150 cycles at a current density of 500 mA/g.²⁸ However, the rate capability and cycling performance still needs more improvements to make it a promising anode candidate for the practical applications.

In this work, we designed and synthesized novel hierarchical $\text{Co}_2\text{V}_2\text{O}_7$ nanosheets consisted of interconnected nanoparticles using graphene oxides (GO) as the template (Figure 1). This unique architecture can provide the following three important features simultaneously: (1) short pathways for Li ions and electrons provided by two-dimensional nanostructure and reduced particle size, (2) sufficient voids for the volume

Received: November 26, 2015

Accepted: January 11, 2016

Published: January 11, 2016

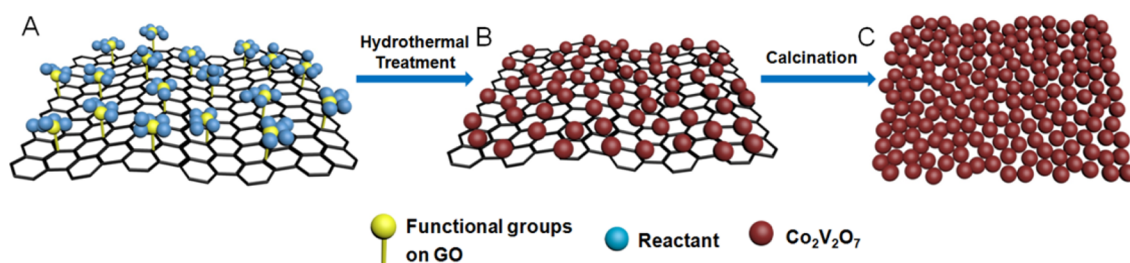


Figure 1. Schematic diagram of the experimental technique for growing hierarchical CoVO-1 nanosheets. (A) CoVO-1 nanosheet precursor before hydrothermal treatment. (B) CoVO-1 nanosheet precursor after hydrothermal treatment. (C) CoVO-1 nanosheet after calcination treatment.

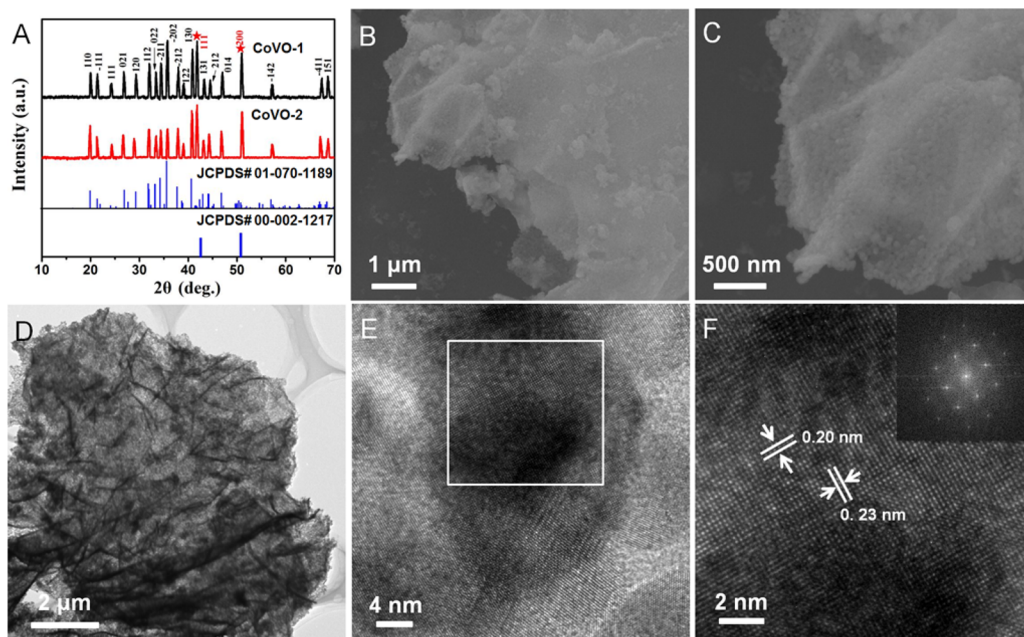


Figure 2. (A) XRD patterns of CoVO-1 and CoVO-2. (B–C) SEM images of CoVO-1. (D–F) TEM and HRTEM images and FFT pattern of CoVO-1.

expansion/extraction during the electrochemical processes, and (3) rapid ion transport enabled by electrolyte-filled mesoporous network. As the anode material for LIBs, the hierarchical $\text{Co}_2\text{V}_2\text{O}_7$ nanosheets exhibit a high reversible specific capacity (962 mAh/g at 0.5 A/g), excellent rate capability, and long cycle life (441 mAh/g after 900 cycles at 5.0 A/g).

2. EXPERIMENTAL SECTION

Synthesis of Hierarchical $\text{Co}_2\text{V}_2\text{O}_7$ Nanosheets. The hierarchical $\text{Co}_2\text{V}_2\text{O}_7$ nanosheets were synthesized by a hydrothermal process followed by calcination in air. In a typical synthesis process, 4 mL of GO solution (prepared via a modified Hummer's method, 1 mg/mL) was dispersed in 40 mL distilled water and stirred for 1 h. 1.495 g of cobalt acetate ($\text{Co}(\text{CH}_3\text{COO})_2 \cdot 4\text{H}_2\text{O}$) was then added directly into the GO solution and stirred for another 1 h. Subsequently, 0.702 g of ammonium vanadate (NH_4VO_3) was dissolved in deionized water with stirring at 80 °C for 15 min. The obtained transparent NH_4VO_3 solution was added into the GO and cobalt acetate solution dropwise and stirred for 1 h to form reddish brown suspension. Ethylene glycol (EG) was then added. After 30 min, anhydrous ethylene diamine (EDA) was added; gray precipitate appeared immediately with the addition of EDA. After stirring for 5 h, the gray suspended solution obtained was transferred into a 100 mL Teflon-lined autoclave and hydrothermally treated at 180 °C for 48 h. The resulting products were collected by centrifugation, washed with deionized water and ethanol, and dried at 80 °C in air. Finally, the obtained precursor was sintered at 450 °C for 10 h in air to get the

brown product, which is denoted as CoVO-1. As a control experiment, CoVO-2 was prepared using the same procedure except without the addition of GO template.

Characterization and Electrochemical Measurement. The crystallographic information on CoVO-1 and CoVO-2 were confirmed by X-ray powder diffraction (XRD, Bruker D8 Discover) with nonmonochromated Co $K\alpha$ X-ray source. The morphologies of CoVO-1 and CoVO-2 were characterized by field emission scanning electron microscope (FESEM, JEOL JSM-7100F) and high-resolution transmission electron microscope (HRTEM, JEOL JEM-2100F, 200 kV). The specific surface area and Barrett–Joyner–Halenda (BJH) pore size distribution were analyzed using Micromeritics Tristar 3020 instrument.

The electrochemical performance was evaluated via CR2025-type coin cell on a LAND battery testing system (CT2001A, China). To make the working electrode, the 70 wt % active material (CoVO-1 and CoVO-2) and 20 wt % acetylene black (Super-P) were mixed with 10 wt % sodium alginate (dissolve in deionized water to form 2.5 wt % aqueous solution) to form slurries. Then, the slurries were coated onto copper foil and dried at 120 °C overnight under air. The obtained electrode was punched into circular disks with an average mass loading of active material of 2 mg/cm². The lithium foil was used as the anodes and 1 M LiPF_6 in ethylene carbon (EC)/dimethyl carbonate (DMC) with a volume ratio of 1:1 was used as the electrolyte. Before the discharge/charge processes, the cells were aged for 12 h to ensure full absorption of the electrolyte into the electrodes. Galvanostatic discharge/charge tests were performed in the voltage range of 0.01–2.50 V under constant current mode. Cyclic voltammetry (CV) tests

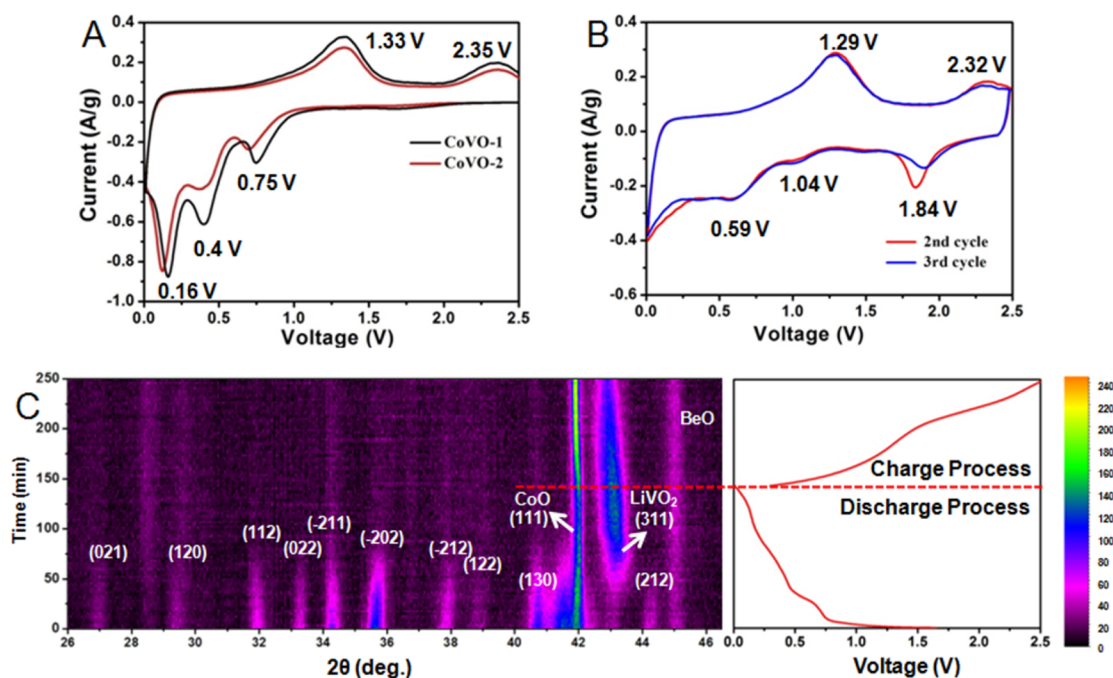


Figure 3. (A) The first cycle of cyclic voltammetry curves of CoVO-1 and CoVO-2 at a sweep rate of 0.1 mV/s in the potential range from 0.01 to 2.5 V vs Li/Li⁺. (B) The second and third cycles of cyclic voltammetry curves of CoVO-1 at a sweep rate of 0.1 mV/s in the potential range from 0.01 to 2.5 V vs Li/Li⁺. (C, left) In situ X-ray diffraction patterns of CoVO-1 and (right) corresponding discharge/charge curve.

were carried out on a CHI 760D electrochemical workstation. The electrochemical impedance spectroscopy (EIS) was tested using the Autolab PGSTAT 302N electrochemical workstation at the cell voltage of 2.2 V in the frequency range from 100 kHz to 0.01 Hz. All the tests were performed at room temperature.

For in situ XRD measurement, the 70% active materials were grounded with 20% acetylene black and 10% poly(tetrafluoroethylene) (PTFE) to get circular electrode disks, then the electrode was placed in the specific cell with an X-ray-transparent beryllium window, which also acts as a current collector. During the charge/discharge process, the in situ XRD signals were collected directly using the planar detector under still mode, and each pattern took 2 min to acquire. The schematic diagram of the in situ cell is exhibited as Figure S1.

3. RESULTS AND DISCUSSION

Figure 2A shows the X-ray diffraction (XRD) patterns of the as-prepared hierarchical Co₂V₂O₇ nanosheets (CoVO-1) and the control sample synthesized without template (CoVO-2). For both materials, the majority of the diffraction peaks can be indexed to monoclinic Co₂V₂O₇ (JCPDS Card No. 01-070-1189, space group *P21/n*), while two residual peaks from cubic CoO (marked by stars, JCPDS Card No. 00-002-1217, space group *Fm $\bar{3}$ m*) can also be observed. CoVO-1 presents a typical sheet-like morphology (Figure 2B,C), which is inherited from the GO template. Each nanosheet consists of numerous interconnected primary nanoparticles. The primary particle size is 30–50 nm, and the clear voids between neighboring nanoparticles can be clearly observed according to the transmission electron microscopic (TEM) images (Figure 2D). Typical high-resolution TEM images of CoVO-1 are shown in Figure 2E,F. The (014) and (024) lattice fringes of monoclinic Co₂V₂O₇, with atomic spacings of 0.23 and 0.20 nm respectively, can be clearly discerned. EDS results show that the Co, V, and O coexist in the sample and the Co/V ratio is around 1.14 (Figures S2 and S3, Table S1), indicating the molar concentration of CoO in the mixture is about 22%. Elemental analysis is applied to determine the residual amount

of carbon content in the CoVO-1 material, the detail data is listed in Table S2. On the basis of the experimental data, it is obvious that the residual carbon is negligible in the final sample (the average amount of carbon is 0.035% in total), indicating the graphene oxide is completely removed after the calcination procedure. For the purpose of comparison, CoVO-2, without the addition of GO template, is also prepared. Similar to CoVO-1, CoVO-2 is also comprised of primary nanoparticles (Figure S4A,B). However, according to the TEM image, the Co₂V₂O₇ nanoparticles aggregate severely into irregular shapes without the help of GO template (Figure S4C).

The porous properties of CoVO-1 and CoVO-2 have been studied by nitrogen adsorption. Both samples show a type IV isotherm with distinct capillary condensation and hysteresis loop at a high relative pressure of 0.75–1.0 (Figure S5). According to the pore size distribution curve, both of the concrete pore sizes are in the distribution of 2–20 nm with an average pore size of 12 nm, which are consistent with the TEM results. However, the CoVO-1 shows a slightly higher BET specific surface area (27.6 m²/g) than that of CoVO-2 (24.9 m²/g), which could be attributed to the hierarchical nanosheet structure of CoVO-1 with less aggregation.

Meanwhile, the existence of GO during the synthesis process is the key factor for the major morphology difference between CoVO-1 and CoVO-2. Here, GO is considered as an ideal template for the nucleation and growth of nanocrystals because of its two-dimensional (2D) structure, oxygen-containing functional groups on the surface, and good mechanical properties (Figure S6A).^{29–31} Ethylene glycol (EG) is a common chelating agent to limit the particle growth and ensure the dispersity of nanoparticles. Ethylene diamine (EDA) has a stronger chelating effect for transition-metal ions, which would influence the crystal growth.³² Both EG and EDA can act as surfactants to modify the surface of GO and significantly lower the nucleation energy, resulting in the dense nucleation

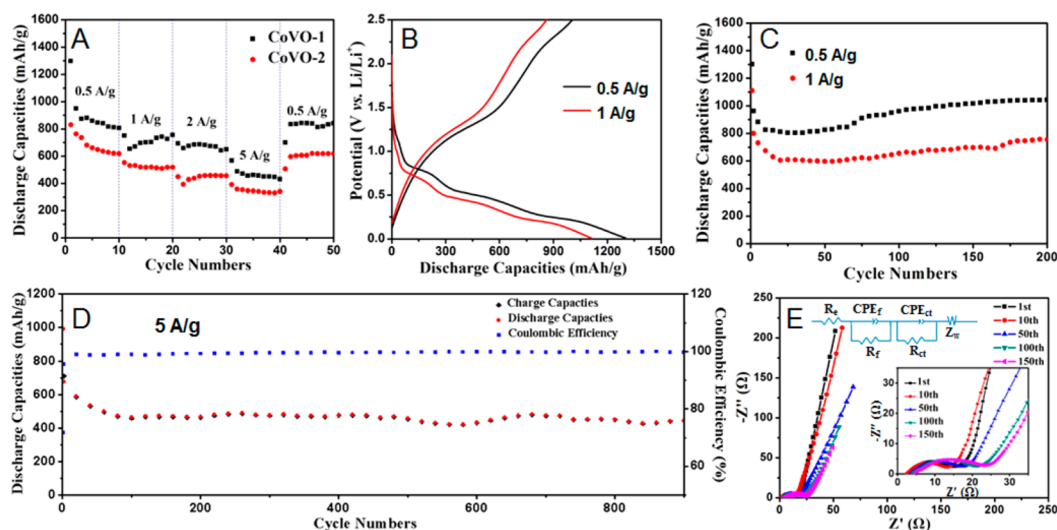


Figure 4. (A) Discharge capacities of CoVO-1 and CoVO-2 at various rates from 0.5 to 5.0 A/g. (B) The first discharge/charge curves of CoVO-1 at different current densities. (C) The detailed cycling performance of the CoVO-1 at different current densities. (D) Electrochemical properties of CoVO-1 at high rate of 5.0 A/g for 900 cycles. (E) The typical Nyquist plots of CoVO-1 after different cycles.

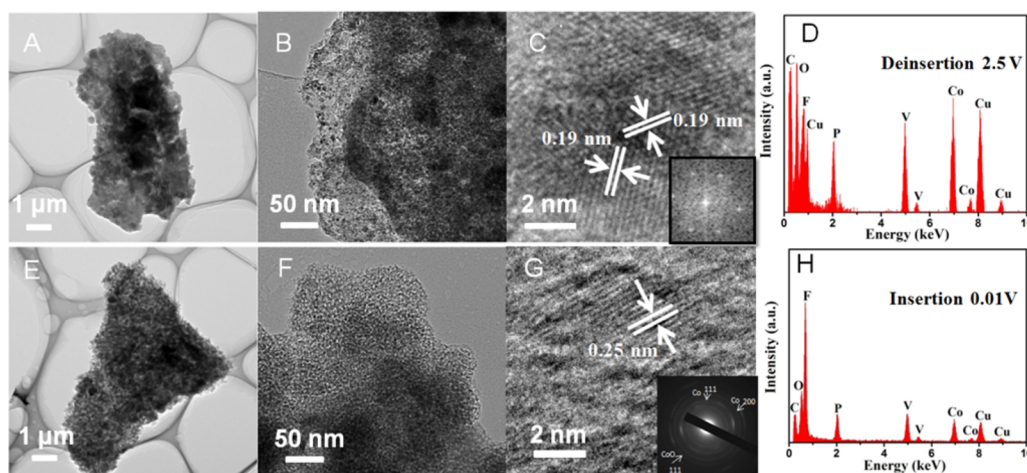


Figure 5. (A–D) Ex situ TEM images and corresponding EDS result collected at the voltage of 2.5 V after 10 cycles. (E–H) Ex situ TEM images and corresponding EDS result collected at the voltage of 0.01 V after 10 cycles.

of nanocrystals on GO.³³ During the hydrothermal process, the initial nuclei gradually grow, forming well-crystallized nanocrystals (Figure S6B). The gases produced by the oxidation of GO and organics would form vacancies, which further condense into large mesopores. This method allows the duplication of the GO template surface to form the nanosheet morphology.

The lithium storage behaviors of CoVO-1 and CoVO-2 are investigated by cyclic voltammetry (CV) analysis at a scan rate of 0.1 mV/s in the potential window of 0.01–2.5 V (Figure 3A,B and Figure S7). Both samples exhibit similar CV curves, implying the identical electrochemical reaction. However, CoVO-1 has higher redox currents, larger curve area, and lower overpotential than CoVO-2, suggesting the higher capacity and faster kinetics for Li-ions diffusion.^{34,35} The initial CV curve is quite different from those of the subsequent cycles (Figure 3B and Figure S7). This phenomenon is due to the irreversible decomposition of electrolyte and destroying of the $\text{Co}_2\text{V}_2\text{O}_7$ crystal structure during the first cycle, which is further demonstrated by the in situ XRD results.

The as-prepared in situ cell is discharged to 0.01 V and then charged to 2.5 V under a constant current of 500 mA/g at 25 °C. The discharge curve contains three plateaus, matching well with the initial CV curve (Figure 3C). The first plateau at 0.75 V is accompanied by the slight decrease in $\text{Co}_2\text{V}_2\text{O}_7$ peak intensity. Besides the decrease in peak intensity, no other changes can be observed in the XRD pattern, suggesting that the first plateau at 0.75 V might be associated with the formation of solid electrolyte interface (SEI). The second plateau at 0.4 V is accompanied by the disappearance of $\text{Co}_2\text{V}_2\text{O}_7$ diffraction peaks and the emergence of a new peak at 43° (Figure 3C). The new peak at 43° can be indexed to the (311) diffraction peak of LiVO_2 . This is further confirmed by the appearance of new peaks at 21.5 and 51.5° , corresponding to the (111) and (400) planes of LiVO_2 (Figure S8). Thus, it is speculated that the second plateau is associated the decomposition of $\text{Co}_2\text{V}_2\text{O}_7$ ($\text{Co}_2\text{V}_2\text{O}_7 = 2 \text{Co} + \text{V}_2\text{O}_5$) and the lithiation of V_2O_5 ($\text{V}_2\text{O}_5 + 4 \text{Li}^+ + 4 \text{e}^- \rightarrow 2 \text{LiVO}_2 + 2\text{Li}_2\text{O}$). Upon further lithiation, the reactions at around 0.16 V correspond to the formation of metallic Co from CoO nanoparticles and lithiation of LiVO_2 ($\text{LiVO}_2 + x\text{Li}^+ + xe^-$

→ $\text{Li}_{1+x}\text{VO}_2$).^{12,36} The conventional in situ XRD pattern array has been presented as Figure S9. During the subsequent charge process, two oxidation peaks located at 1.33 and 2.35 V can be observed, which are ascribed to the formation of CoO from metallic Co and the delithiation of the vanadium oxides.¹³ In the lithium intercalation process of the following cycles, three cathodic peaks are observed at 1.84, 1.04, and 0.59 V, respectively (Figure 3B). The electrochemical reactions are very similar to that of the $\text{Co}_3\text{V}_2\text{O}_8$ reported previously,²¹ demonstrating the reversible transformation between Co and CoO, combining with the emergence of lithiated/delithiated vanadium oxide.

Figure 4A shows the rate performance of CoVO-1 and CoVO-2 from 0.5 to 5.0 A/g. It is clear that the CoVO-1 exhibits a good cycling response at various current densities. The average capacities are 961, 709, 669, 457 mAh/g at 0.5, 1.0, 2.0, and 5.0 A/g, respectively. When the current density is reduced from 5.0 to 0.5 A/g, a capacity of 833 mAh/g can be recovered for the CoVO-1. CoVO-2 exhibits a lower rate capability, further confirming the advantage of our rationally designed CoVO-1 hierarchical nanosheets.

Figure 4B presents the first cycle discharge/charge curves at 0.5 and 1.0 A/g of CoVO-1. Three discharge plateaus can be observed, in accordance with the CV results. The initial discharge capacity is 1301 mAh/g at 0.5 A/g and 1110 mAh/g at 1.0 A/g. Figure 4C shows the cycling performances of CoVO-1 at 0.5 and 1.0 A/g. High reversible capacities of 962 and 799 mAh/g can be achieved at current densities of 0.5 and 1.0 A/g, respectively. An interesting phenomenon appears during the cycling performance test is that the capacity increases gradually with cycle number after the initial decrease; similar phenomenon has been reported previously.^{10,11,21,37} The initial capacity decrease might be attributed to the deconstruction of $\text{Co}_2\text{V}_2\text{O}_7$ structure, the formation of solid electrolyte interphase (SEI), and side reactions.^{21,37} Meanwhile, the active material is not fully utilized, which is confirmed by the coexistence of CoO and Co at the voltage of 0.01 V in Figure 5G. Along with further cycling, the unused active material would take part in the electrochemical reaction, resulting in increased capacity.

We further investigated the long-life cycling performance of the CoVO-1, which exhibits a desirable cycling performance (Figure 4D). A reversible discharge capacity of 677 mAh/g can be achieved at the rate of 5.0 A/g, which is comparable to the reported Co–V-based mixed metal oxides. Notably, even after 900 cycles, a capacity of 441 mAh/g can still be obtained. This is the longest cycle life for cobalt vanadium oxide electrode materials to our best knowledge.^{21,25–28} The corresponding voltage capacity profiles at the cycle of 1, 2, 10, 100, 200, 500, and 900 are exhibited in Figure S10. Moreover, their Coulombic efficiency is stabilized at above 99% after 30 cycles, indicating the efficient transport of electrons and ions in the anode. The capacity fluctuation during the long-cycling test can be attributed to the small temperature fluctuation of the environment, as all the tests were performed at room temperature. The superior electrochemical performance could be attributed to the following reasons: (1) The voids between primary particles provide short pathways for Li ions diffusion and sufficient spaces for the volume expansion/extraction during the electrochemical processes.^{1,34,38–40} (2) The formation of uniform and stable SEI resulted from the hierarchical $\text{Co}_2\text{V}_2\text{O}_7$ nanosheet structure would increase the reversible capacity and Coulombic efficiency.^{41,42}

The detailed reaction kinetics of the CoVO-1 at the voltage of 2.2 V after different cycles was investigated using electrochemical impedance spectroscopy (EIS) in the frequency range of 100 kHz to 0.01 Hz. The equivalent circuit is exhibited in Figure 4E, which contains equivalent series resistance (R_e), SEI resistance (R_f), and charge transfer resistance (R_{ct}). Meanwhile, CPE_f and CPE_{ct} are the capacitance related to SEI and the double layer, while Z_w corresponds to the ion diffusion in the active material.⁴³ The semicircle part has been enlarged as the inset figure in Figure 4E. It is worth noting that only one semicircle is observed initially, while two depressed semicircles at high and middle frequencies begin to appear with the increasing cycles. This phenomenon is associated with the formation of SEI layer on the surface of active materials. Moreover, it is interesting to note that the R_{ct} encounters a first decrease and then increase with the increasing number of cycles, as shown in Figure 4E and Table S3. The initial decreased R_{ct} could be attributed to the activation process, as the electrochemical reaction helps to improve the contact between the electrolyte and the electrode, resulting in the reduced interfacial impedance of the fresh electrode.⁴⁴ However, the R_{ct} grows gradually along with the cycling process, as the crystal $\text{Co}_2\text{V}_2\text{O}_7$ has transformed into smaller CoO particles and vanadium oxide associated with forming SEI,¹³ which may increase the grain boundary and lower the conductivity of the electrodes. Afterward, SEI becomes uniform and stable with the further cycling, which is beneficial for the lithium ion transport. This speculation is confirmed by the EIS plot after 100 and 150 cycles, as they show a very similar feature. The experimental phenomenon indicates the electron conduction and ion diffusion pathways in the composite electrodes are well maintained after certain cycles, leading to good cycling stability during the electrochemical process.

In order to find out the reason to the superior electrochemical performance, ex situ TEM was conducted to characterize the morphological and structural changes at 2.5 V (Figure 5A–D) and 0.01 V (Figure 5E–H) after 10 cycles. It is obvious that the nanosheet morphology is well preserved during the electrochemical tests (Figure 5A,E), which can be attributed to the uniformly distributed pores in the original hierarchical $\text{Co}_2\text{V}_2\text{O}_7$ nanosheet to accommodate the volume expansion during cycling.¹⁸ After the lithium intercalation at 2.5 V, the obtained nanoparticles are well distributed and attached on the amorphous matrix (Figure 5C). The interlayer distances of 0.19 nm can be ascribed to the CoO (200) layer. After the lithium deintercalation at 0.01 V, the nanosheet is composed of numerous quantum dots, which are the mixture of metallic Co and CoO, according to the FFT pattern (Figure 5G). Besides, the interlayer distance of crystal structure is 0.25 nm, corresponding to the (111) lattice fringe of CoO, indicating the incomplete conversion from CoO to Co. The appearance of F and P in Figure 5D,H can result from the formation of SEI. The SEM images of hierarchical $\text{Co}_2\text{V}_2\text{O}_7$ nanosheet after 100 cycles have been exhibited as Figure S11, which still present a typical nanosheet structure, indicating the integrity and stability of the as-synthesized material after cycling test.

4. CONCLUSION

In summary, the electrochemical reaction mechanism of the novel hierarchical $\text{Co}_2\text{V}_2\text{O}_7$ nanosheet anode is thoroughly investigated by in situ XRD and ex situ TEM. The results reveal that the initial $\text{Co}_2\text{V}_2\text{O}_7$ transforms into CoO nanoparticles and

LiVO₂ in the first cycle, while the following conversion reaction mainly occurs between CoO and Co and lithiation/delithiation of the vanadium oxides. The resulting nanosized CoO and Co are firmly anchored on the vanadium oxide nanosheets, which could provide the shortened Li-ion/electron diffusion pathway, and avoid structural degradation caused by lithium insertion/extraction, ensuring a good rate capability and high cycling stability. This novel hierarchical Co₂V₂O₇ nanosheet anode exhibits a high reversible capacity (962 mAh/g at 0.5 A/g), remarkable rate capability, and good cycling stability (a capacity of 441 mAh/g can still be obtained after 900 discharge/charge cycles at 5.0 A/g). Our work indicates that this hierarchical Co₂V₂O₇ nanosheet anode is one of the most promising anodes for the practical applications.

■ ASSOCIATED CONTENT

Supporting Information

The Supporting Information is available free of charge on the ACS Publications website at DOI: 10.1021/acsami.5b11510.

Energy-dispersive X-ray spectroscopy (EDS) and elemental analysis results of CoVO-1. The influence of graphene on the morphology and electrochemical performance of the products were investigated by XRD, SEM, TEM, BET, CV, in situ X-ray and EIS. (PDF)

■ AUTHOR INFORMATION

Corresponding Author

* E-mail: mlq518@whut.edu.cn.

Author Contributions

These authors contributed equally to this work.

Notes

The authors declare no competing financial interest.

■ ACKNOWLEDGMENTS

This work was supported by the National Basic Research Program of China (2013CB934103, 2012CB933003), the International Science & Technology Cooperation Program of China (2013DFA50840), National Natural Science Foundation of China (51521001, 51272197), and the National Natural Science Fund for Distinguished Young Scholars (51425204), and the Fundamental Research Funds for the Central Universities (WUT: 2015-III-021, 2015-III-032). Thanks to Prof. C. M. Lieber of Harvard University and Prof. Dongyuan Zhao of Fudan University for strong support and stimulating discussion.

■ REFERENCES

- (1) Jia, X. L.; Cheng, Y. H.; Lu, Y. F.; Wei, F. Building Robust Carbon Nanotube-Interweaved-Nanocrystal Architecture for High-Performance Anode Materials. *ACS Nano* **2014**, *8*, 9265–9273.
- (2) Larcher, D.; Tarascon, J. M. Towards Greener and More Sustainable Batteries for Electrical Energy Storage. *Nat. Chem.* **2015**, *7*, 19–29.
- (3) An, Q. Y.; Wei, Q. L.; Zhang, P.; Sheng, J. Z.; Hercule, K. M.; Lv, F.; Wang, Q. Q.; Wei, X. J.; Mai, L. Q. Three-Dimensional Interconnected Vanadium Pentoxide Nanonetwork Cathode for High-Rate Long-Life Lithium Batteries. *Small* **2015**, *11*, 2654–2660.
- (4) Raju, V.; Wang, X. F.; Luo, W.; Ji, X. L. Multiple Ambient Hydrolysis Deposition of Tin Oxide into Nanoporous Carbon to Give a Stable Anode for Lithium-Ion Batteries. *Chem. - Eur. J.* **2014**, *20*, 7686–7691.

- (5) Luo, Y. Z.; Xu, X.; Zhang, Y. X.; Pi, Y. Q.; Yan, M. Y.; Wei, Q. L.; Tian, X. C.; Mai, L. Q. Three-Dimensional LiMnPO₄·Li₃V₂(PO₄)₃/C Nanocomposite as a Bicontinuous Cathode for High-Rate and Long-Life Lithium-Ion Batteries. *ACS Appl. Mater. Interfaces* **2015**, *7*, 17527–17534.

- (6) Lv, D. P.; Gordin, M. L.; Yi, R.; Xu, T.; Song, J. X.; Jiang, Y. B.; Choi, D.; Wang, D. H. GeO_x/Reduced Graphene Oxide Composite as an Anode for Li-Ion Batteries: Enhanced Capacity via Reversible Utilization of Li₂O along with Improved Rate Performance. *Adv. Funct. Mater.* **2014**, *24*, 1059–1066.

- (7) Ko, M.; Chae, S.; Jeong, S.; Oh, P.; Cho, J. Elastic *a*-Silicon Nanoparticle Backboned Graphene Hybrid as a Self-Compacting Anode for High-Rate Lithium Ion Batteries. *ACS Nano* **2014**, *8*, 8591–8599.

- (8) Jian, Z. L.; Zheng, M. B.; Liang, Y. L.; Zhang, X. X.; Gheyhani, S.; Lan, Y. C.; Shi, Y.; Yao, Y. Li₃VO₄ Anchored Graphene Nanosheets for Long-Life and High-Rate Lithium-Ion batteries. *Chem. Commun.* **2015**, *51*, 229–231.

- (9) Bai, J.; Li, X. G.; Liu, G. Z.; Qian, Y. T.; Xiong, S. L. Unusual Formation of ZnCo₂O₄ 3D Hierarchical Twin Microspheres as a High-Rate and Ultralong-Life Lithium-Ion Battery Anode Material. *Adv. Funct. Mater.* **2014**, *24*, 3012–3020.

- (10) Gao, G. X.; Yu, L.; Wu, H. B.; Lou, X. W. D. Hierarchical Tubular Structures Constructed by Carbon-Coated α -Fe₂O₃ Nanorods for Highly Reversible Lithium Storage. *Small* **2014**, *10*, 1741–1745.

- (11) An, Q. Y.; Lv, F.; Liu, Q. Q.; Han, C. H.; Zhao, K. N.; Sheng, J. Z.; Wei, Q. L.; Yan, M. Y.; Mai, L. Q. Amorphous Vanadium Oxide Matrixes Supporting Hierarchical Porous Fe₃O₄/Graphene Nanowires as a High-Rate Lithium Storage Anode. *Nano Lett.* **2014**, *14*, 6250–6256.

- (12) Peng, C. X.; Chen, B. D.; Qin, Y.; Yang, S. H.; Li, C. Z.; Zuo, Y. H.; Liu, S. Y.; Yang, J. H. Facile Ultrasonic Synthesis of CoO Quantum Dot/Graphene Nanosheet Composites with High Lithium Storage Capacity. *ACS Nano* **2012**, *6*, 1074–1081.

- (13) Huang, G. Y.; Xu, S. M.; Lu, S. S.; Li, L. Y.; Sun, H. Y. Micro-/Nanostructured Co₃O₄ Anode with Enhanced Rate Capability for Lithium-Ion Batteries. *ACS Appl. Mater. Interfaces* **2014**, *6*, 7236–7243.

- (14) Wang, C.; Li, Q.; Wang, F. F.; Xia, G. F.; Liu, R. Q.; Li, D. Y.; Li, N.; Spindelov, J. S.; Wu, G. Morphology-Dependent Performance of CuO Anodes via Facile and Controllable Synthesis for Lithium-Ion Batteries. *ACS Appl. Mater. Interfaces* **2014**, *6*, 1243–1250.

- (15) Ni, J. F.; Zhao, Y.; Li, L.; Mai, L. Q. Ultrathin MoO₂ Nanosheets for Superior Lithium Storage. *Nano Energy* **2015**, *11*, 129–135.

- (16) Sun, Y. M.; Hu, X. L.; Luo, W.; Xia, F. F.; Huang, Y. H. Reconstruction of Conformal Nanoscale MnO on Graphene as a High-Capacity and Long-Life Anode Material for Lithium Ion Batteries. *Adv. Funct. Mater.* **2013**, *23*, 2436–2444.

- (17) Zhou, X. L.; Zhong, Y. R.; Yang, M.; Zhang, Q.; Wei, J. P.; Zhou, Z. Co₂(OH)₂CO₃ Nanosheets and CoO Nanonets with Tailored Pore Sizes as Anodes for Lithium Ion Batteries. *ACS Appl. Mater. Interfaces* **2015**, *7*, 12022–12029.

- (18) Wang, X. H.; Fan, Y.; Susantyoko, R. A.; Xiao, Q. Z.; Sun, L. M.; He, D. Y.; Zhang, Q. High Areal Capacity Li Ion Battery Anode Based on Thick Mesoporous Co₃O₄ Nanosheet Networks. *Nano Energy* **2014**, *5*, 91–96.

- (19) Wu, H.; Xu, M.; Wang, Y. C.; Zheng, G. F. Branched Co₃O₄/Fe₂O₃ Nanowires as High Capacity Lithium-Ion Battery Anodes. *Nano Res.* **2013**, *6*, 167–173.

- (20) Jadhav, H. S.; Kalubarme, R. S.; Park, C. N.; Kim, J.; Park, C. J. Facile and Cost Effective Synthesis of Mesoporous Spinel NiCo₂O₄ as an Anode for High Lithium Storage Capacity. *Nanoscale* **2014**, *6*, 10071–10076.

- (21) Yang, G. Z.; Cui, H.; Yang, G. W.; Wang, C. X. Self-Assembly of Co₃V₂O₈ Multilayered Nanosheets: Controllable Synthesis, Excellent Li-Storage Properties, and Investigation of Electrochemical Mechanism. *ACS Nano* **2014**, *8*, 4474–4487.

- (22) Liu, B.; Zhang, J.; Wang, X. F.; Chen, G.; Chen, D.; Zhou, C. W.; Shen, G. Z. Hierarchical Three-Dimensional ZnCo₂O₄ Nanowire

Arrays/Carbon Cloth Anodes for a Novel Class of High-Performance Flexible Lithium-Ion Batteries. *Nano Lett.* **2012**, *12*, 3005–3011.

(23) Yu, L.; Zhang, L.; Wu, H. B.; Zhang, G. Q.; Lou, X. W. Controlled Synthesis of Hierarchical $\text{Co}_x\text{Mn}_{3-x}\text{O}_4$ Array Micro-/Nanostructures with Tunable Morphology and Composition as Integrated Electrodes for Lithium-Ion Batteries. *Energy Environ. Sci.* **2013**, *6*, 2664–2671.

(24) Zhu, J.; Xu, Z.; Lu, B. G. Ultrafine Au Nanoparticles Decorated NiCo_2O_4 Nanotubes as Anode Material for High-Performance Supercapacitor and Lithium-Ion Battery Applications. *Nano Energy* **2014**, *7*, 114–123.

(25) Baudrin, E.; Laruelle, S.; Denis, S.; Touboul, M.; Tarascon, J. M. Synthesis and Electrochemical Properties of Cobalt Vanadates vs. Lithium. *Solid State Ionics* **1999**, *123*, 139–153.

(26) Denis, S.; Baudrin, E.; Orsini, F.; Ouvrard, G.; Touboul, M.; Tarascon, J. M. Synthesis and Electrochemical Properties of Numerous Classes of Vanadates. *J. Power Sources* **1999**, *81–82*, 79–84.

(27) Tang, Y.; Zhou, J.; Liu, J.; Liu, L. X.; Liang, S. Q.; Li, Y. Facile Synthesis of Cobalt Vanadium Oxides and Their Applications in Lithium Batteries. *Mater. Lett.* **2013**, *8*, 1138–1145.

(28) Wu, F. F.; Yu, C. H.; Liu, W. X.; Wang, T.; Feng, J. K.; Xiong, S. L. Large-Scale Synthesis of $\text{Co}_2\text{V}_2\text{O}_7$ Hexagonal Microplatelets under Ambient Conditions for Highly Reversible Lithium Storage. *J. Mater. Chem. A* **2015**, *3*, 16728–16736.

(29) Tan, C. L.; Huang, X.; Zhang, H. Synthesis and Applications of Graphene-Based Noble Metal Nanostructures. *Mater. Today* **2013**, *16*, 29–36.

(30) Yan, Y.; Yin, Y. X.; Guo, Y. G.; Wan, L. J. A Sandwich-Like Hierarchically Porous Carbon/Graphene Composite as a High-Performance Anode Material for Sodium-Ion Batteries. *Adv. Energy Mater.* **2014**, *4*, 1301584.

(31) Ou, X. W.; Gan, L.; Luo, Z. T. Graphene-Templated Growth of Hollow Ni_3S_2 Nanoparticles with Enhanced Pseudocapacitive Performance. *J. Mater. Chem. A* **2014**, *2*, 19214–19220.

(32) Sun, C. W.; Rajasekhara, S.; Goodenough, J. B.; Zhou, F. Monodisperse Porous LiFePO_4 Microspheres for a High Power Li-Ion Battery Cathode. *J. Am. Chem. Soc.* **2011**, *133*, 2132–2135.

(33) Li, X. L.; Qi, W.; Mei, D. H.; Sushko, M. L.; Aksay, I.; Liu, J. Functionalized Graphene Sheets as Molecular Templates for Controlled Nucleation and Self-Assembly of Metal Oxide-Graphene Nanocomposites. *Adv. Mater.* **2012**, *24*, 5136–5141.

(34) Xu, X.; Luo, Y. Z.; Mai, L. Q.; Zhao, Y. L.; An, Q. Y.; Xu, L.; Hu, F.; Zhang, L.; Zhang, Q. J. Topotactically Synthesized Ultralong LiV_3O_8 Nanowire Cathode Materials for High-Rate and Long-Life Rechargeable Lithium Batteries. *NPG Asia Mater.* **2012**, *4*, e20.

(35) Guo, Y.; Huang, Y. D.; Jia, D. Z.; Wang, X. C.; Sharma, N.; Guo, Z. P.; Tang, X. C. Preparation and Electrochemical Properties of High-Capacity $\text{LiFePO}_4\text{-Li}_3\text{V}_2(\text{PO}_4)_3/\text{C}$ Composite for Lithium-Ion Batteries. *J. Power Sources* **2014**, *246*, 912–917.

(36) Wu, Z. S.; Ren, W. C.; Wen, L.; Gao, L. B.; Zhao, J. P.; Chen, Z. P.; Zhou, G. M.; Li, F.; Cheng, H. M. Graphene Anchored with Co_3O_4 Nanoparticles as Anode of Lithium Ion Batteries with Enhanced Reversible Capacity and Cyclic Performance. *ACS Nano* **2010**, *4*, 3187–3194.

(37) Zhang, N.; Zhao, Q.; Han, X. P.; Yang, J. G.; Chen, J. Pitaya-Like $\text{Sn}@\text{C}$ Nanocomposites as High-Rate and Long-Life Anode for Lithium-Ion Batteries. *Nanoscale* **2014**, *6*, 2827–2832.

(38) Sun, H. T.; Xin, G. Q.; Hu, T.; Yu, M. P.; Shao, D. L.; Sun, X.; Lian, J. High-Rate Lithiation-Induced Reactivation of Mesoporous Hollow Spheres for Long-Lived Lithium-Ion Batteries. *Nat. Commun.* **2014**, *5*, 4526.

(39) Ding, Y. L.; Wen, Y. R.; Wu, C.; van Aken, P. A.; Maier, J.; Yu, Y. 3D V_6O_{13} Nanotextiles Assembled from Interconnected Nanogrooves as Cathode Materials for High-Energy Lithium Ion Batteries. *Nano Lett.* **2015**, *15*, 1388–1394.

(40) Li, L.; Wang, H. Q.; Fang, X. S.; Zhai, T. Y.; Bando, Y.; Golberg, D. High-Performance Schottky Solar Cells using ZrS_2 Nanobelt Networks. *Energy Environ. Sci.* **2011**, *4*, 2586–2590.

(41) Guo, B. K.; Yu, X. Q.; Sun, X. G.; Chi, M. F.; Qiao, Z. A.; Liu, J.; Hu, Y. S.; Yang, X. Q.; Goodenough, J. B.; Dai, S. A Long-Life Lithium-Ion Battery with a Highly Porous TiNb_2O_7 Anode for Large-Scale Electrical Energy Storage. *Energy Environ. Sci.* **2014**, *7*, 2220–2226.

(42) Liu, N.; Lu, Z. D.; Zhao, J.; McDowell, M. T.; Lee, H. W.; Zhao, W. T.; Cui, Y. A Pomegranate-Inspired Nanoscale Design for Large-Volume-Change Lithium Battery Anodes. *Nat. Nanotechnol.* **2014**, *9*, 187–192.

(43) Ji, H. X.; Zhang, L. L.; Pettes, M. T.; Li, H. F.; Chen, S. S.; Shi, L.; Piner, R.; Ruoff, R. S. Ultrathin Graphite Foam: A Three-Dimensional Conductive Network for Battery Electrodes. *Nano Lett.* **2012**, *12*, 2446–2451.

(44) Li, M. L.; Yang, X.; Wang, C. Z.; Chen, N.; Hu, F.; Bie, X. F.; Wei, Y. J.; Du, F.; Chen, G. Electrochemical Properties and Lithium-Ion Storage Mechanism of LiCuVO_4 as an Intercalation Anode Material for Lithium-Ion Batteries. *J. Mater. Chem. A* **2015**, *3*, 586–592.